The Use of the Transfinite Interpolation in the Method of Moments Applied to Electromagnetic Scattering by Dielectric Cylinders

Philippe De Doncker

***Abstract*—The method of moments (MoM) solution of electromagnetic scattering presents two major numerical difficulties: the number of unknowns and the computation time necessary to calculate the matrix elements. To circumvent these problems, a MoM using the transfinite interpolation and a reduced integration scheme is presented here. The so-called h and p versions of the new method are applied to the scattering of an electromagnetic wave by an infinite dielectric cylinder (TM case) in the Richmond's formulation. The transfinite and classical methods are compared in terms of the convergence rates of the radar cross section and of the total electric field inside the dielectric. The results confirm the superiority of the new schemes as predicted by the theory.**

***Index Terms*—Electromagnetic scattering, integral equations, interpolation, moment methods, numerical analysis.**

I. Introduction

MANY electromagnetic applications require the analysis of the scattering of a wave by a conducting or dielectric cylinder. In this kind of problems, the domain of interest is infinite and the numerical solution is often carried out using the method of moments (MoM) [1] to solve integral equations which automatically incorporate the Sommerfeld radiation condition. However, these methods result in a full matrix representation and the large number of unknowns necessary to obtain accurate results represents a major numerical difficulty. The MoM is commonly referred as a low-frequency method since its use is generally restricted to bodies that are not large in terms of the wavelength.

The MoM solution of electromagnetic scattering generally involves the subdivision of the scatterer in small elements called patches or cells. In each cell the unknown field is approximated in terms of simple interpolation functions. An approach to reduce the computational needs could be to improve the efficiency of this interpolation process. Following this idea, the use of the *transfinite interpolation* [2] is presented here.

The transfinite interpolation (TFI) theory is a mathematical tool originally developed for the geometrical problems of computer-aided design (CAD) and numerically controlled machining of free-form surfaces such as automobile exterior panels. Rapidly it has been adapted and applied to the problem of curvilinear mesh generation for finite element analysis [15] and it is now become a standard method for surface and volume modeling (see [17] for an introduction to this technique or [19], [20] and references therein for its last developments). But the use of the TFI has not been restricted to CAD. Thanks to its special properties, it has made possible to develop curvilinear finite difference schemes in fluid mechanics [16] or finite-element methods, which satisfy natural boundary conditions exactly [18]. All these applications are based on the link between TFI and geometrical modeling. But the TFI presents another powerful feature which is more barely known: for the same interpolation functions degree, it leads to a much better accuracy than the classical interpolation as it will be shown further and it could thus be useful to decrease the huge computational needs of the MoM.

The idea of enhancing the performances of the MoM by using more elaborate interpolation basis is not new. In the first developments of the volume integral equations based MoM, pulse functions were considered in both two and three dimensions [3], [8], [10]. However, it rapidly appeared that this kind of approximation is not efficient and that it leads to the presence of spurious surface charge densities inside the scatterer [8]. To circumvent this problem, numerical techniques have been developed using the so-called rooftop functions on cells of various shapes [11]–[14]. More recently, to still enhance the accuracy of the MoM, the use of isoparametric elements has been proposed [4]. All of those methods are efficient but none of the authors insists on the crucial role played by the interpolation process, which is never studied separately from the geometrical modeling which is also become more and more elaborate. Moreover, in applications such as in biomedical engineering the use of simple discretization grids could be preferable on one hand to simplify the very difficult mesh generation task and on the other hand to be easily compatible with the algebraic systems solvers optimized by the fast Fourier transform (FFT) algorithm. The TFI theory fills in this gap by presenting a general formalism to study and to enhance the performances of the interpolation process.

To the author's knowledge, it is the first time the transfinite interpolation is explicitly used in the MoM. However, a particular case of the p version presented here leads to the interpolation basis used in the isoparametric elements yet studied in [4]. The

Manuscript received May 4, 1998; revised September 3, 1999.

The author is with the Département d'Electricité Générale, Faculté des Sciences Appliquées, Université Libre de Bruxelles, CP165/51 Elecgen, 1050 Bruxelles, Belgium.

Publisher Item Identifier S 0018-926X(00)01649-5.

theory presented here is more general than the isoparametric elements interpolation theory and it emphasizes the leading part of the interpolation scheme itself in the MoM solution of integral equations.

II. Operator Formulation of the Method of Moments

Let us consider the canonical problem

$$\mathcal{L}\,\phi(x,y,z) = Q(x,y,z) \tag{1}$$

where $\mathcal{L}$ is an integro-differential operator defined on a volume V, $\phi(x,y,z)$ is the unknown function (which could eventually represents a component of a vectorial field) and $Q(x,y,z)$ is the source term.

In the MoM, the first step to convert this problem into an algebraic system is to divide the volume V in small cells (the case of entire domain basis functions is not considered here). In each cell c an approximation $\tilde{\phi}_c(x,y,z)$ of the unknown $\phi(x,y,z)$ is defined in terms of simple interpolation functions and of the value of ϕ at the interpolation nodes (x_l^c, y_m^c, z_n^c) of the cell

$$\tilde{\phi}_c(x,y,z) = \sum_{l=1}^{L}\sum_{m=1}^{M}\sum_{n=1}^{N} \cdot \phi(x_l^c, y_m^c, z_n^c)\, u_l^c(x) v_m^c(y) w_n^c(z) \tag{2}$$

where $\{u_l^c\}$, $\{v_m^c\}$ and $\{w_n^c\}$ are basis functions spanning finite dimensional linear spaces and are nonzero only over the volume of the cell c.

Substituting (2) into (1), and summing over the cells dividing V, we obtain the *discretized equation*:

$$\mathcal{L}\sum_{c=1}^{N_c}\tilde{\phi}_c(x,y,z) = Q(x,y,z) \tag{3}$$

where N_c is the total number of cells.

In order to write this equation in an operator formulation, let P_x^c, P_y^c and P_z^c be the one dimensional interpolation operators defined for any function $f(x,y,z)$ by

$$\begin{aligned} P_x^c f(x,y,z) &= \sum_{l=1}^{L} u_l^c(x) f(x_l^c, y, z) \\ P_y^c f(x,y,z) &= \sum_{m=1}^{M} v_m^c(y) f(x, y_m^c, z) \\ P_z^c f(x,y,z) &= \sum_{n=1}^{N} w_n^c(z) f(x, y, z_n^c). \end{aligned} \tag{4}$$

For instance, the operator P_x^c associated with the linear interpolation in x on a segment $[0,h]$ is defined by

$$P_x^c f(x,y,z) = f(0,y,z)\,\frac{h-x}{h} + f(h,y,z)\,\frac{x}{h}. \tag{5}$$

Readily, the operators P_x^c, P_y^c, and P_z^c are commutative $(P_x^c P_y^c = P_y^c P_x^c, \cdots)$ and if the basis functions satisfy the cardinality condition

$$u_m^c(x_n^c) = v_m^c(y_n^c) = w_m^c(z_n^c) = \delta_{mn} \quad \forall m,n \tag{6}$$

they are projectors, i.e., linear idempotent operators ($P_x^{c2} = P_x^c$, $P_y^{c2} = P_y^c$, and $P_z^{c2} = P_z^c$). Substituting (4) into (2) the approximation $\tilde{\phi}_c(x,y,z)$ of $\phi(x,y,z)$ in each cell can thus be viewed in this case as a projection called the *tensor-product* projection of $\phi(x,y,z)$

$$\tilde{\phi}_c(x,y,z) = P_x^c P_y^c P_z^c\,\phi(x,y,z) \tag{7}$$

and the discretized problem (3) takes the form

$$\mathcal{L}\sum_c P_x^c P_y^c P_z^c\,\phi(x,y,z) = Q(x,y,z). \tag{8}$$

Clearly, the projection process (7) of ϕ on a finite-dimensional space is a crucial step for the global accuracy of the numerical solution. Generally, pulse functions or piecewise linear (rooftop) functions are chosen to span this projection space. By enhancing the precision of the projection we could expect a better efficiency of the numerical process, i.e., to use less unknowns with the same global accuracy.

III. Transfinite Method of Moments

The transfinite interpolation will be very concisely presented in this section without proofs. All the details of this theory can be found, e.g., in [2] and [5].

From (6) and (7) it can be easily shown that the accuracy set of the projection (defined as the set of points where the interpolant $\tilde{\phi}_c$ equals the original function ϕ) is formed by the nodes (x_l^c, y_m^c, z_n^c)

$$\tilde{\phi}_c(x_l^c, y_m^c, z_n^c) = \phi(x_l^c, y_m^c, z_n^c). \tag{9}$$

On the other hand, we can consider another approximation $\pi_c(x,y,z)$ of $\phi(x,y,z)$ obtained by application of the *boolean sum* projection

$$\pi_c(x,y,z) = (P_x^c \oplus P_y^c \oplus P_z^c)\phi(x,y,z) \tag{10}$$

where the boolean sum of two commutative operators A, B is defined as

$$(A \oplus B)\phi = (B \oplus A)\phi = (A + B - AB)\phi. \tag{11}$$

The accuracy set of $\pi_c(x,y,z)$ is formed by the *surfaces* (x_l^c, y, z), (x, y_m^c, z), (x, y, z_n^c). This accuracy set thus, consists of an infinite number of points, whence the name of *transfinite interpolation* (TFI). This property is the starting point of the application of the TFI in volume or surface modeling. With (11), (10) can be explicitly written as

$$\begin{aligned} \pi_c(x,y,z) = &(P_x^c + P_y^c + P_z^c - P_x^c P_y^c - P_x^c P_z^c - P_y^c P_z^c \\ &+ P_x^c P_y^c P_z^c)\phi(x,y,z). \end{aligned} \tag{12}$$

Of course, to obtain an algebraic system, only point values of $\phi(x,y,z)$ can appear in the interpolant and a *second level* interpolation is necessary for the terms of (12), which does not contain the three projections in x, y, and z. This results in a new interpolant $\tilde{\pi}_c$ of ϕ

$$\begin{aligned} \tilde{\pi}_c(x,y) = &(\tilde{P}_y^c \tilde{P}_z^c P_x^c + \tilde{P}_x^c \tilde{P}_z^c P_y^c + \tilde{P}_x^c \tilde{P}_y^c P_z^c \\ &- \tilde{P}_z^c P_x^c P_y^c - \tilde{P}_y^c P_x^c P_z^c - \tilde{P}_x^c P_y^c P_z^c \\ &+ P_x^c P_y^c P_z^c)\phi(x,y,z) \end{aligned} \tag{13}$$

where $\tilde{P}_x^c$, $\tilde{P}_y^c$ and $\tilde{P}_z^c$ are the second level interpolation projectors. The discretized version (3) of the original problem now takes the formulation

$$\mathcal{L}\sum_c (P_x^c\tilde{P}_y^c\tilde{P}_z^c + \tilde{P}_x^c P_y^c \tilde{P}_z^c + \tilde{P}_x^c\tilde{P}_y^c P_z^c - P_x^c P_y^c \tilde{P}_z^c - P_x^c\tilde{P}_y^c P_z^c - \tilde{P}_x^c P_y^c P_z^c + P_x^c P_y^c P_z^c)\phi(x,y,z) = Q(x,y,z). \quad (14)$$

It is the so-called *transfinite MoM* formulation of the original problem.

Let P_x^c, P_y^c, and P_z^c correspond to Lagrange interpolation with polynomials of degree k on cells of sides h. The superiority of the transfinite scheme comes from the fact that asymptotically when $h \to 0$, the interpolation errors associated with the transfinite projection (10) and with the classical projection (7) are given, respectively, by [5]

$$\varepsilon_{tfi} \sim \mathcal{O}(h^{3k+3}) \qquad \varepsilon_{cl} \sim \mathcal{O}(h^{k+1}). \quad (15)$$

The accuracy order of the first-level transfinite scheme is thus three times that of the classical scheme using interpolation functions of the same degree.

In the transfinite case, the second-level interpolations have to be chosen so that they do not degrade the accuracy order of the first-level interpolation. This can be achieved in two different ways. In the so-called h version, the second-level interpolation is chosen of the same degree as the first level, but on a finer grid. In the so-called p version, the second-level interpolation is of a higher degree on the same grid. Let $\tilde{P}_x^c$, $\tilde{P}_y^c$, and $\tilde{P}_z^c$ be the second-level projectors corresponding to Lagrange interpolation of degree l on segments of width $\overline{h}$. In the h version $(l = k)$ the second-level grid is to be chosen so that asymptotically [5]

$$\overline{h} = h^3. \quad (16)$$

And in the p version $(\overline{h} = h)$ the second-level interpolation degree must satisfy [5]

$$l = 3k + 2. \quad (17)$$

It is important to note that the only constraint the interpolation operators have to satisfy is to be commutative projectors. The transfinite scheme is thus very general and can be used with a lot of interpolation methods. We will restrict ourselves here to the study of the transfinite MoM using Lagrange basis functions, but it is obvious that in other electromagnetic applications it can be generalized for instance to trigonometric or spline interpolations.

In the two-dimensional (2-D) case, the transfinite interpolant is given by

$$\pi_c(x,y) = (P_x^c \oplus P_y^c)\phi(x,y) \quad (18)$$

and the interpolation errors are

$$\varepsilon_{tfi} \sim \mathcal{O}(h^{2k+2}) \qquad \varepsilon_{cl} \sim \mathcal{O}(h^{k+1}). \quad (19)$$

The second-level interpolant can now be written as

$$\tilde{\pi}_c(x,y) = (\tilde{P}_y^c P_x^c + \tilde{P}_x^c P_y^c - P_x^c P_y^c)\phi(x,y) \quad (20)$$

where the second-level interpolation must satisfy

$$\overline{h} = h^2 \quad (21)$$

in the h version and

$$l = 2k + 1 \quad (22)$$

in the p version.

IV. Application to the Scattering By a Dielectric Cylinder

Thanks to the theory outlined in the previous section, it is possible to apply the TFI on volume integrals representations of three-dimensional (3-D) scatttering problems. However, to validate our approach it is much easier from the computational complexity point of view to first solve the 2-D problem of the scattering by a inhomogeneous lossy dielectric cylinder. The TFI has been applied with success for both the TM and TE cases in combination with the volume-surface integral equation (VSIE) developed by Jin *et al.* [21], [22]. But here, for conciseness without losing the key features of the TFI, only TM results will be presented. The original formulation developed by Richmond [3] to solve this problem will be used to solve for the scattered field and the induced field inside the dielectric. In the following sections of this paper, the time dependence $e^{j\omega t}$ is understood.

Let the incident electric field be $\vec{E}_i = E_i\,\vec{1}_z$ where the z axis is taken parallel with the axis of the cylinder. The cylinder material is assumed to be linear, isotropic, to have a constant permeability μ_0 and an inhomogeneous complex relative permittivity $\epsilon_r(x,y)$. Let $\vec{E} = E\vec{1}_z$ be the total field and $\vec{E}_s = E_s\vec{1}_z$ the scattered field. From the fact that

$$E = E_i + E_s \quad (23)$$

Richmond has shown that the integral equation for the total field is

$$E(x,y) + \frac{jk_0^2}{4}\int_S (\epsilon_r - 1)E(x',y')H_0^{(2)}(k_0\rho)\,dx'\,dy' = E_i(x,y) \quad (24)$$

where S is the cross section of the cylinder, k_0 is the free-space wave number and ρ is defined as

$$\rho = \sqrt{(x-x')^2 + (y-y')^2}. \quad (25)$$

In the original work of Richmond, the cylinder cross section was divided in square cells and the total electric field E was supposed to be constant in each cell. In the operator formulation, it is, in fact, the 2-D equivalent of the tensor-product projection (7) with P_x^c and P_y^c the projectors on constant basis functions. Fig. 1(a) shows the interpolation node associated with this interpolation. Let ε_R be the interpolation error of this method. Since $P_x^c P_y^c \phi$ is in this case a zero-order polynomial approximation, for a cell of size h the order of ε_R is thus given asymptotically when $h \to 0$ by (see (19)):

$$\varepsilon_R = \mathcal{O}(h). \quad (26)$$

Finally, to obtain an algebraic system, the point-matching procedure at the interpolation nodes was used.

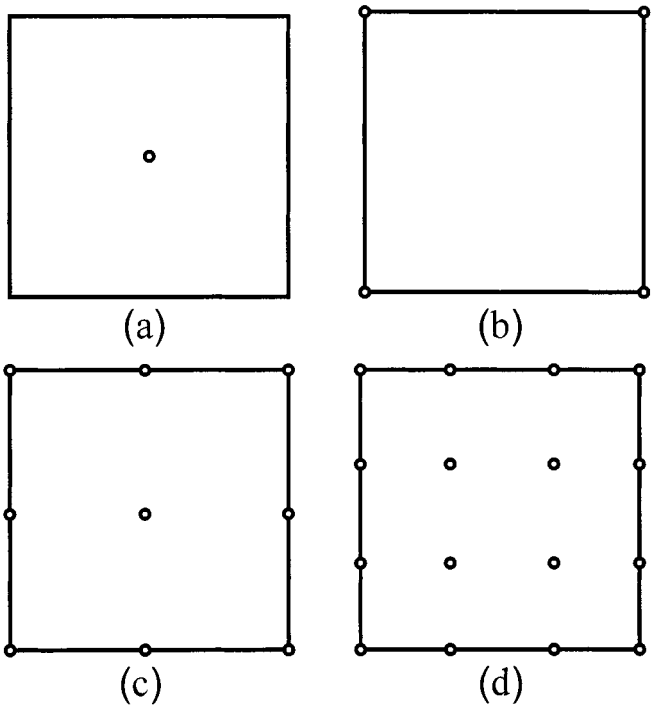

Fig. 1. Interpolation cells and nodes corresponding to the classical (a) pulse; (b) linear; (c) quadratic; and (d) cubic interpolations.

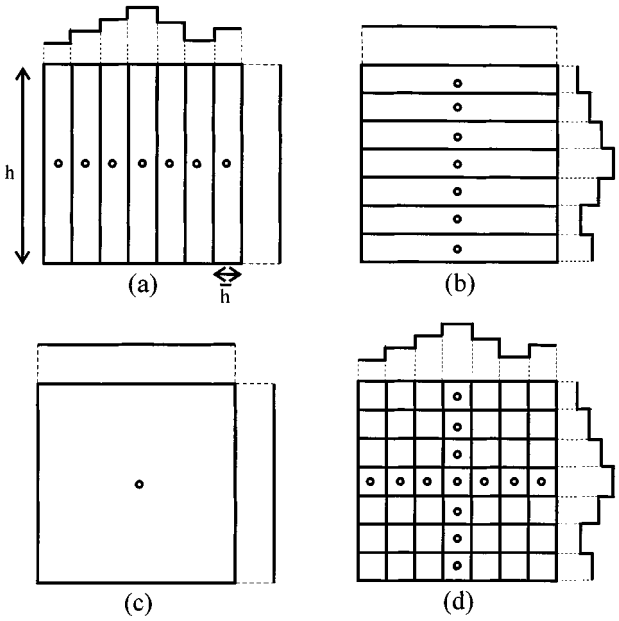

Fig. 2. Nodes, cells, and interpolation functions shapes corresponding to each term of the transfinite h version. (a) Term $\tilde{P}_x^c P_y^c$. (b) Term $P_x^c \tilde{P}_y^c$. (c) $P_x^c P_y^c$. (d) Global transfinite interpolant.

A. The Transfinite h Version

In this version, pulse functions are used for both the first- and second-level interpolations in (20). Let P_x^c and P_y^c be the projectors on constant basis functions of width h. Let $\tilde{P}_x^c$ and $\tilde{P}_y^c$ be the second-level interpolation projectors on constant basis functions of width $\overline{h}$. To keep the first-level interpolation accuracy, asymptotically, when $h \to 0$, (21) must hold and, in this case, the order of the interpolation error called ε_h is given by (19)

$$\varepsilon_h = \mathcal{O}(h^2). \tag{27}$$

Using only pulse functions, the interpolation accuracy order is twice the Richmond's one. Fig. 2 shows the interpolation nodes and cells corresponding to the three terms of (20) and to the global transfinite interpolant $\tilde{\pi}_c(x, y)$. In the transfinite case, each *macro-cell* of size h is divided in horizontal and vertical *micro-cells* of width $\overline{h}$, the number of micro-cells depending on the macro-cell size following (21). The term $P_x^c P_y^c E$ corresponds to the classical piecewise constant approximation on cells of size h. The terms $\tilde{P}_x^c P_y^c E$ and $\tilde{P}_y^c P_x^c E$ correspond to the classical approximation on one axis and to the finer approximation on cells of width $\overline{h}$ on the other one. As shown by Fig. 2(d), the transfinite h version uses in each macro-cell a piecewise constant approximation of the unknown function on micro-cells of size $\overline{h}$, which is obtained thanks to only a few interpolation nodes. Of course, there are much more unknowns per macro-cell in the transfinite scheme than in the Richmond's one. However, substituting (21) into (27) gives

$$\varepsilon_h = \mathcal{O}(\overline{h}). \tag{28}$$

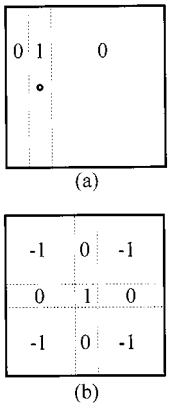

Fig. 3. Basis functions of the transfinite h version for (a) the lateral node and (b) the central node.

Hence, considering (26), to obtain the same global accuracy with the Richmond's formulation, it would be necessary to use cells of size $\overline{h}$. As shown by Fig. 2(d), the transfinite h version yields thus an important gain in the number of unknowns keeping the same kind of basis functions. Using (20) it is easy to write the basis functions associated with each node of Fig. 2(d). These functions are given on Fig. 3 in the case of a macro-cell divided in 7×7 micro-cells (case of Fig. 2). Since they are essentially pulse functions, the practical implementation of the h version does not present any special difficulty compared to the Richmond's formulation.

B. Transfinite p Versions

Let P_x and P_y be the projectors on the one-dimensional (1-D) Lagrange linear interpolation functions, i.e., for a cell $\Omega_c[0,h]\times[0,h]$

$$P_x^c E(x,y) = E(0,y)\,\frac{h-x}{h} + E(h,y)\,\frac{x}{h}$$
$$P_y^c E(x,y) = E(x,0)\,\frac{h-y}{h} + E(x,h)\,\frac{y}{h}. \tag{29}$$

In the classical formulation, the use of rooftop functions can be considered as a tensor-product $P_x^c P_y^c$ projection with the associated error given by $\mathcal{O}(h^2)$. On the other hand, the first-level transfinite interpolant is given by (18)

$$\begin{aligned}(P_x^c \oplus P_y^c)E(x,y) &= E(0,y)\,\frac{h-x}{h} + E(h,y)\,\frac{x}{h} + E(x,0)\,\frac{h-y}{h} \\ &\quad + E(x,h)\,\frac{y}{h} - E(0,0)\,\frac{h-y}{h}\,\frac{h-x}{h} \\ &\quad - E(0,h)\,\frac{y}{h}\,\frac{h-x}{h} - E(h,0)\,\frac{h-y}{h}\,\frac{x}{h} \\ &\quad - E(h,h)\,\frac{x}{h}\,\frac{y}{h}.\end{aligned} \tag{30}$$

To obtain only point values of $E(x,y)$, the terms $E(0,y)$, $E(h,y)$, $E(x,0)$, and $E(x,h)$ need a second-level interpolation. Thanks to the first equation of (19), with $k=1$ the order of accuracy of the first-level interpolation is $\mathcal{O}(h^4)$. The second-level projectors have to be chosen to not degrade this accuracy.

In a first step, let $\tilde{P}_x^c$ and $\tilde{P}_y^c$ be interpolation projectors on the 1-D quadratic Lagrange interpolation functions on a segment $[0,h]$

$$\begin{aligned}\tilde{P}_x E(x,y) &= \frac{(x-h/2)(x-h)}{h^2/2}\,E(0,y) \\ &\quad + \frac{x(h-x)}{h^2/4}\,E(h/2,y) + \frac{x(x-h/2)}{h^2/2}\,E(h,y) \\ \tilde{P}_y E(x,y) &= \frac{(y-h/2)(y-h)}{h^2/2}\,E(x,0) \\ &\quad + \frac{y(h-y)}{h^2/4}\,E(x,h/2) + \frac{y(y-h/2)}{h^2/2}\,E(x,h).\end{aligned} \tag{31}$$

The order of accuracy of each of these second level interpolations is $\mathcal{O}(h^3)$, smaller than the first-level one, and determines thus the order of the global 2-D interpolation error ε_{pq}

$$\varepsilon_{pq} = \mathcal{O}(h^3). \tag{32}$$

Using (20), (30), and (31), it is easy to compute the basis functions belonging to each node of the transfinite interpolation cell. Their analytical expressions are given in Appendix A. Fig. 4 shows the interpolation nodes corresponding to each term of (20) and to the global interpolant $\tilde{\pi}_c(x,y)$ and Fig. 1(c) those of the classical quadratic interpolation (which is in fact the tensor-product projection $\tilde{P}_x^c \tilde{P}_y^c E(x,y)$ and has the same interpolation error $\mathcal{O}(h^3)$). It appears that only eight interpolation nodes belong to each cell. The term $P_x^c P_y^c E$ corresponds to the classical piecewise linear approximation on cells of size h. The terms $\tilde{P}_x^c P_y^c E$ and $\tilde{P}_y^c P_x^c E$ correspond to the linear approximation on one axis and to the quadratic approximation on the other one. On an average, in the transfinite quadratic scheme there are three nodes per cell (taking into account the fact that the nodes are common to adjacent cells) and in the classical quadratic scheme four nodes per cell. The gain in unknowns is thus 25%. Furthermore, the reduced integration scheme presented in the next section is only applicable to the transfinite basis. The second-level quadratic interpolation scheme is not the optimal choice, but is a good tradeoff between complexity and accuracy.

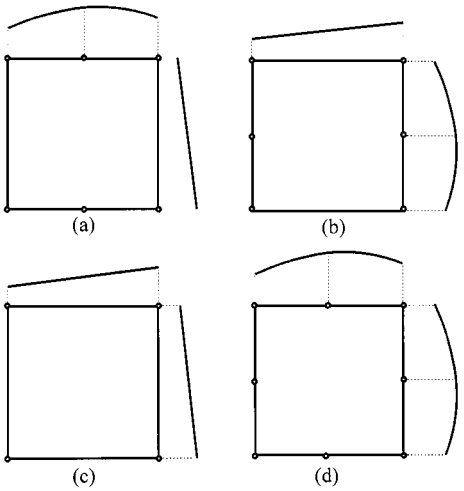

Fig. 4. Interpolation nodes and interpolation functions shapes corresponding to each term of the quadratic transfinite p version. (a) Term $P_x^c P_y^c$. (b) Term $P_x^c \tilde{P}_y^c$. (c) $P_x^c P_y^c$. (d) Global interpolant.

The elements shown in Fig. 4 are the same as the isoparametric elements used in [4]. However, the approach presented here is quite different, it can be generalized to other kinds of interpolations and it also shows that the choice of quadratic elements is not the optimal one from the interpolation point of view.

In fact, after (22), the maximal accuracy would be obtained with second-level Lagrange cubic interpolation and in this case the order of the interpolation error ε_{pc} is

$$\varepsilon_{pc} = \mathcal{O}(h^4). \tag{33}$$

Fig. 5 shows the interpolation nodes corresponding to this scheme and Fig. 1(d) those corresponding to the classical cubic interpolation scheme which has the same accuracy order. For conciseness, the analytical expressions of the basis functions are not reproduced here. Each term of (20) has the same structure as in the transfinite quadratic case. On an average, in the transfinite cubic method there are five nodes per cell and in the classical cubic method nine nodes per cell. The gain in unknowns is thus about 45%.

It is unprofitable to use higher order Lagrange interpolation basis for the second-level interpolation. The maximal accuracy order, which can be reached with a first level linear interpolation is given by the first of (19), i.e., $\mathcal{O}(h^4)$. The interpolations

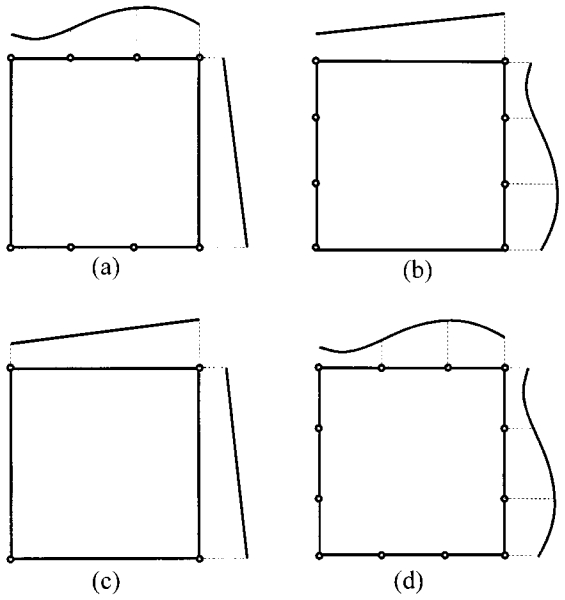

Fig. 5. Interpolation nodes and interpolation functions shapes corresponding to each term of the cubic transfinite p-version. (a) $\bar{P}_x^c P_y^c$. (b) $P_x^c \bar{P}_y^c$. (c) $P_x^c P_y^c$. (d) Global interpolant.

are not to be of the Lagrange type. The same results can be obtained for instance with second-level cubic splines interpolation or first-level trigonometric or exponential interpolations.

All the theory and the applications presented in the previous sections were developed in the case of parallelipipedic or rectangular cells. However, for problems where the geometrical description is a crucial parameter, all the TFI theory can be generalized to the most general curvilinear cells as it is shown in the Appendix B.

V. Reduced Integration Scheme

The transfinite interpolation allows a large reduction of the number of unknowns but a second major numerical difficulty remains: each element of the algebraic system matrix is obtained by integration over the surface of the cell corresponding to the element, which is very time consuming.

Papagiannakis [6] has proposed an integration scheme which reduces in the 3-D case the 3-D volume integrals to 2-D integrals over the surface of the cells or in the 2-D case the 2-D integrals to line integrals over the boundary of the cells (if the permittivity is supposed to be constant in the cell). However, this scheme is only applicable in the case of pulse functions interpolation and it is used here in the h version of the transfinite MoM. It will be shown that thanks to the properties of the transfinite basis, a reduced integration scheme can also be found in the 2-D quadratic or cubic p version of the transfinite method.

In the p version, the transfinite approximation $\tilde{E}_c(\vec{r})$ of $E(\vec{r})$ in each interpolation cell c can be written

$$\tilde{E}_c(\vec{r}) = \sum_{k=1}^{K} E_{c,k}\, \xi_k(\vec{r}) \tag{34}$$

where $E_{c,k}$ is the value of $E(\vec{r})$ at the node k of the cell c, K is the number of nodes belonging to cell c ($K = 8$ in the quadratic case and $K = 12$ in the cubic case) and $\xi_k(\vec{r})$ is the interpolation function corresponding to the node k and which is nonzero only over the surface Ω_c of the cell c.

Considering (34) and using the point matching at the interpolation nodes, the integral equation (24) becomes

$$E_m + \sum_{c=1}^{N_c} (\epsilon_c - 1) \sum_{k=1}^{K} E_{c,k} \cdot \int_{\Omega_c} k_0^2\, G(\vec{r}_m, \vec{r}')\, \xi_k(\vec{r}')\, d\vec{r}' = E_{im} \qquad m = 1 \cdots N_n \tag{35}$$

where N_c is the total number of cells, N_n is the total number of nodes, ϵ_c is the relative permittivity of cell c (supposed to be constant in the cell), E_m and E_{im} are the values of $E(\vec{r})$ and $E_i(\vec{r})$ at the node m (located on $\vec{r}_m$), and $G(\vec{r}, \vec{r}')$ is defined as

$$G(\vec{r}, \vec{r}') = \frac{j}{4} H_0^{(2)}(k_0 \rho) \qquad \rho = \sqrt{(x - x')^2 + (y - y')^2}. \tag{36}$$

The problem is thus to reduce the surface integral

$$\int_{\Omega_c} k_0^2\, G(\vec{r}_m, \vec{r}')\, \xi_k(\vec{r}')\, d\vec{r}' \tag{37}$$

to an integration over the the boundary $\partial\Omega_c$ of Ω_c.

Since $G(\vec{r}, \vec{r}')$ is the free-space 2-D Green's function, it satisfies

$$(\Delta' + k_0^2)\, G(\vec{r}, \vec{r}') = \delta(\vec{r} - \vec{r}') \tag{38}$$

where Δ' corresponds to the primed coordinates. The integral (37) is split into two parts

$$\int_{\Omega_c} k_0^2\, G(\vec{r}_m, \vec{r}')\xi_k(\vec{r}')\, d\vec{r}' = \int_{\Omega_c} \xi_k(\vec{r}')(\Delta' + k_0^2)\, G(\vec{r}_m, \vec{r}')\, d\vec{r}' + \int_{\Omega_c} \xi_k(\vec{r}')(-\Delta')G(\vec{r}_m, \vec{r}')\, d\vec{r}'. \tag{39}$$

Considering (38), the first integral of the right member of (39) is solved analytically [7]

$$\int_{\Omega_c} \xi_k(\vec{r}')(\Delta' + k_0^2)\, G(\vec{r}_m, \vec{r}')\, d\vec{r}' = \frac{\Omega_0}{2\pi}\, \xi_k(\vec{r}_m)\, \delta_m^c \tag{40}$$

where Ω_0 is the angle under which the node m sees the cell c ($\Omega_0 = \pi/2$ if m is on a vertice of c, $\Omega_0 = \pi$ if m is on a side of c) and δ_m^c is defined as

$$\delta_m^c = \begin{cases} 1, & \text{if node } m \in \text{cell } c \\ 0, & \text{otherwise.} \end{cases} \tag{41}$$

The second integral of the right member of (39) is solved using the Green's theorem [7]

$$\int_{\Omega_c} \xi_k(\vec{r}')(-\Delta')G(\vec{r}_m,\vec{r}')\,d\vec{r}' = -\int_{\Omega_c} G(\vec{r}_m,\vec{r}')\Delta'\xi_k\,d\vec{r}' + \oint_{\partial\Omega_c}\left(G\,\frac{\partial\xi_k}{\partial n'} - \xi_k\,\frac{\partial G}{\partial n'}\right)dl'. \quad (42)$$

Where the derivatives are taken in the outward direction normal to the cell boundary. The first term of the right member of this equation is the last surface integral remaining. Let $\zeta_k(\vec{r}') = \Delta'\xi_k(\vec{r}')$. Replacing $\Delta'\xi_k$ by ζ_k in (42) exactly the same method as for (37) can be applied on the first term of the right member of this equation. A few manipulations give

$$\int_{\Omega_c} G(\vec{r}_m,\vec{r}')\zeta_k(\vec{r}')\,d\vec{r}' = \frac{1}{k_0^2}\,\frac{\Omega_0}{2\pi}\,\zeta_k(\vec{r}_m)\delta_m^c - \frac{1}{k_0^2}\int_{\Omega_c} G(\vec{r}_m,\vec{r}')\Delta'\zeta_k(\vec{r}')\,d\vec{r}' + \frac{1}{k_0^2}\oint_{\partial\Omega_c}\left(G\,\frac{\partial\zeta_k}{\partial n'} - \zeta_k\,\frac{\partial G}{\partial n'}\right)dl'. \quad (43)$$

Considering the structure of (20), in the p version of the transfinite projection, the term $P_x^c P_y^c$ is linear in both x and y, the term $\tilde{P}_x^c P_y^c$ is linear in y and quadratic or cubic in x and the term $\tilde{P}_y^c P_x^c$ is linear in x and quadratic or cubic in y. Hence, the transfinite interpolation function $\xi_k(\vec{r})$ contains only linear–linear, linear–quadratic, or linear–cubic terms in x and y and consequently

$$\Delta'\zeta_k = \Delta'(\Delta'\xi_k) = 0. \quad (44)$$

The surface integral in (43) is thus vanishing. Let $u_k(\vec{r}')$ be defined as

$$u_k(\vec{r}') = \xi_k(\vec{r}') - \frac{1}{k_0^2}\,\Delta'\xi_k(\vec{r}'). \quad (45)$$

Considering (45), (43), (42), (40) and (39)

$$\int_{\Omega_c} k_0^2 G(\vec{r}_m,\vec{r}')\xi_k(\vec{r}')d\vec{r}' = \frac{\Omega_0}{2\pi}\,u_k(\vec{r}_m)\delta_m^c + \oint_{\partial\Omega_c}\left(G\,\frac{\partial u_k}{\partial n'} - u_k\,\frac{\partial G}{\partial n'}\right)dl' \quad (46)$$

and all the surface integrals have disappeared (the line integrals have to be understood as Cauchy principal value integrals if necessary).

This reduced scheme is only possible if the condition (44) holds, which is not true in the case of the classical quadratic or cubic bivariate interpolation. If $\{\xi_k\}$ are pulse functions, (46) gives the reduced scheme described in [6]. It is worth noting that this reduced scheme can also be used in the VSIE solution of the TE case to remove the surface integrals. A limitation of this reduced scheme is the fact that the permittivity is supposed to be constant in the cell (as it is often considered in practice [3], [6], [10]–[14]) but if the permittivity is supposed to be piecewise constant on subregions of each cell, reduced schemes can be applied separately for each of these subregions.

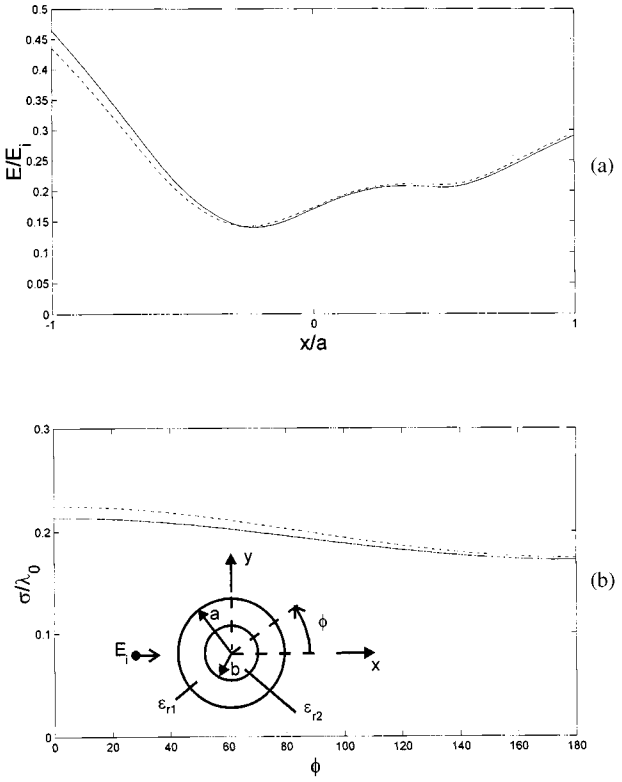

Fig. 6. (a) Analytical results (solid lines) and numerical results (dotted lines) of the normalized electric field along a diameter of the layered muscle-fat cylinder (parallel to the propagation direction) and of the (b) normalized bistatic RCS ($\epsilon_{r1} = 7.5 - j8.64$, $\epsilon_{r2} = 72 - j162$, $a = 0.05\lambda_0$, $b = 0.0263\lambda_0$).

VI. Numerical Results

To validate the new schemes, the transfinite MoM was applied to the scattering of a TM plane wave propagating in the $+x$ direction by a dielectric cylinder. All the numerical simulations presented in this section were obtained with the point-matching procedure and the reduced integration scheme for the transfinite solutions. The algebraic systems were solved for sake of simplicity thanks to the LU decomposition. However, by a good choice of the unknowns numbering (numbering close together equivalent nodes of the different cells) due to the use of the point matching and due to the fact that the interpolation functions are shift invariant from one cell to another, it is possible to see that when the interpolation cells are uniform in the scatterer, the discretization matrix can be written in a block Toeplitz form and it is thus compatible with the iterative solvers using the FFT to evaluate the matrix–vector products (see, e.g., [8], [13]) (In the p version, to obtain the Toeplitz structure, the integral equation must be first written as in (35), i.e., considering nodes common to adjacent cells as several distinct nodes).

Since among the most important applications of the study of the interaction between a dielectric cylinder and an electromagnetic wave are in the biomedical domain, the first example shows the total electric field and bistatic RCS of a layered circular cylinder of radius $0.05\lambda_0$ ($\lambda_0 = 2\pi/k_0$) illuminated by a TM plane wave and whose permittivities and conductivities were chosen to represent a muscle-fat cylinder at 100 MHz [8]. All the h and p versions give results in very good agreement with the analytical solutions and Fig. 6 shows the electric field along

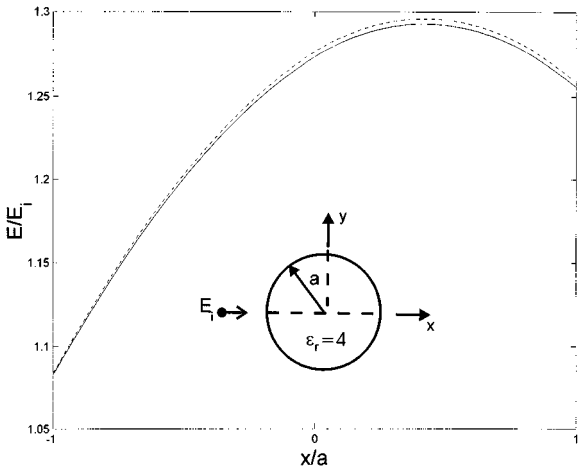

Fig. 7. Analytical result (solid line) and numerical result (dotted line) of the normalized electric field along a diameter of the homogeneous cylinder (parallel to the propagation direction) ($\epsilon_r = 4$, $a = 0.05\lambda_0$).

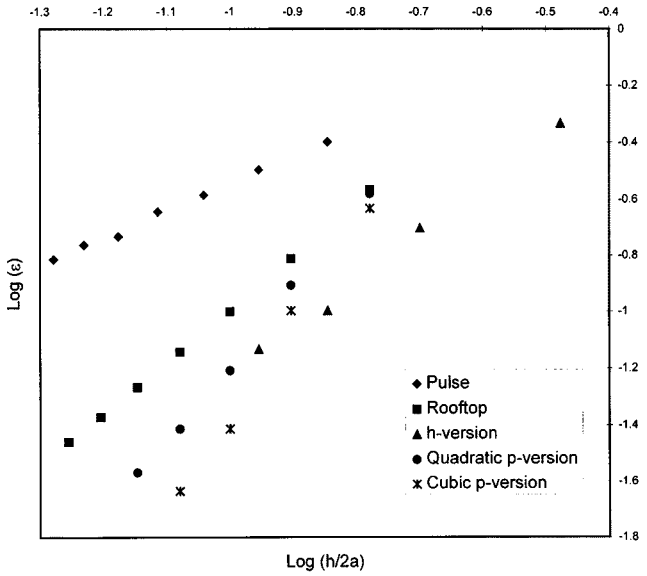

Fig. 8. The rms error ε of the electric field inside a circular dielectric cylinder (radius $a = 0.1\lambda_0$, $\epsilon_r = 54 - j84$) versus the normalized cell size $h/2a$.

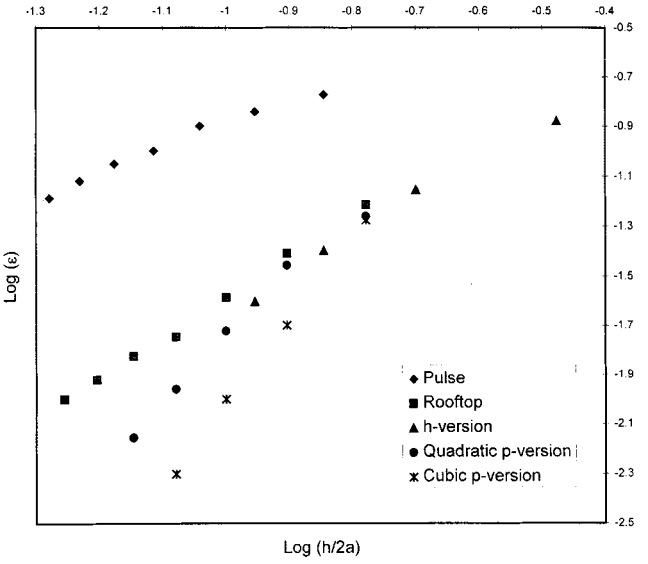

Fig. 9. Supremum error ε of the electric field inside a circular dielectric cylinder (radius $a = 0.1\lambda_0$, ϵ_r = 54-j84) versus the normalized cell size $h/2a$.

a diameter parallel to the x axis of the cylinder obtained with the quadratic p version (with 112 cells) and the bistatic RCS obtained with the h version (with 36 macro cells). The validity of the cubic p version is shown on Fig. 7, which represents the electric field along a diameter parallel to the x axis of an homogeneous cylinder of relative permittivity 4.0 and radius $0.05\lambda_0$ (obtained with 112 cells).

The main advantage of the transfinite versions is a reduction in the number of unknowns. It is necessary to validate the theory by convergence tests. The first test presented here shows the convergence rates of the different methods (the Richmond's and rooftop methods and the h and p versions) concerning the total electric field along a diameter of an homogeneous dielectric circular cylinder of relative permittivity 54.0-j 84.0 and of radius $0.1\lambda_0$. Fig. 8 shows the evolution with the cell size (the macro-cell size for the h version) of the error obtained by the root mean square (rms) norm of the difference between the numerical and the analytical results. The error involved in the Richmond's formulation decreases with a slope 1.0 in the rooftop method with a slope 1.9, in the h version with a slope 1.8, in the quadratic p version with a slope 2.8 and with the cubic p version with a slope 3.5. The superiority of the transfinite schemes is clear and confirms the theory. Fig. 9 shows the same test but with the error calculated with the supremum norm (modulus of the maximal difference between the numerical and analytical results). The slopes are 0.95 for the Richmond's method, 1.7 for the rooftop method, 1.6 for the h version, 2.6 for the quadratic p version, and 3.5 for the cubic p version, which confirms the good behavior of the transfinite MoM.

Since the unknowns number for a given accuracy is smaller in the transfinite than in the classical method, the transfinite scheme seems to be well suited to deal with objects that are of the same order as or larger than the wavelength. In order to compare the different methods concerning larger cylinder scattering and to isolate the effect of the interpolation scheme from the others error sources as the geometrical discretization, the interaction between a TM plane wave and a square cylinder was studied. Figs. 10 and 11 show the convergence of the backscatter cross section with the number of unknowns for an homogeneous square cylinder of side length $2\lambda_0$ ($\varepsilon_r = 4$ and $\varepsilon_r = 2$, respectively) at normal incidence. In this case, no analytical solution exists, but several simulations on smaller cylinders have shown that all the methods converge to the same backscatter cross section and that they are in good agreement with existing numerical results for square cylinders [9]. Again the superiority of the transfinite scheme is clear. For instance on Fig. 11 we see that with 800 unknowns, the transfinite versions are very close from each others and have converged. On the other hand, the Richmond's method gives with the same number of unknowns a backscatter cross section 100% larger. We could expect to solve by the new transfinite MoM problems which are almost intractable with the classical schemes.

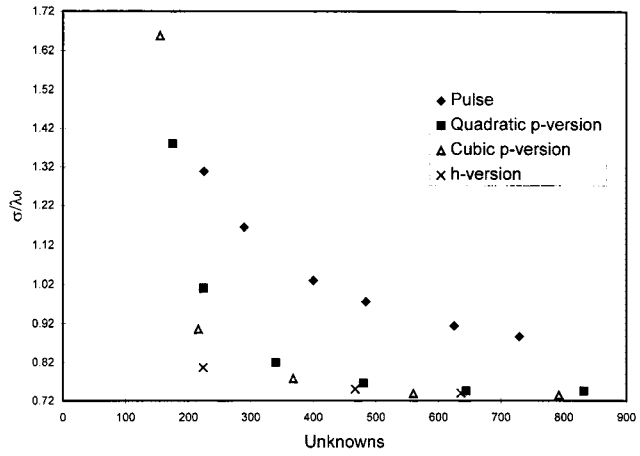

Fig. 10. Convergence of the normalized backscatter cross section with the number of unknowns for a homogeneous square cylinder at normal incidence (side length $= 2\lambda_0, \epsilon_r = 2$).

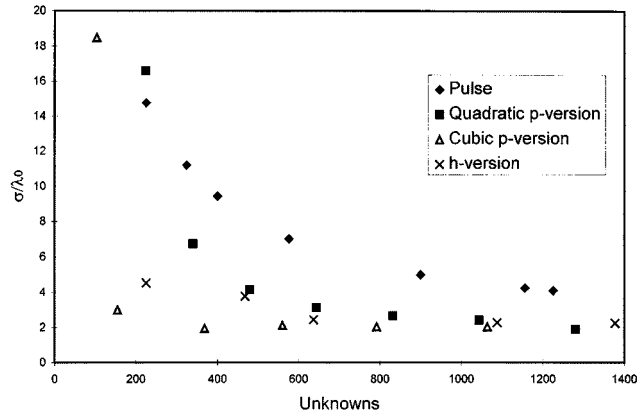

Fig. 11. Convergence of the normalized backscatter cross section with the number of unknowns for a homogeneous square cylinder at normal incidence (side length $= 2\lambda_0, \epsilon_r = 4$).

VII. Conclusion

In this paper, a new kind of MoM was presented based on the use of the transfinite interpolation. After writing the classical MoM in an operator formulation, it was shown how to introduce the transfinite interpolation schemes. Following the nature of the second-level interpolation, the so-called h and p versions of the transfinite MoM were presented and they were shown to give higher accuracy orders with less interpolation nodes than the classical methods. Thanks to the properties of the transfinite basis, a 2-D integration scheme was developed which reduces the surface integrals over the interpolation cells to line integrals over the boundary of the cells. Finally, the efficiency of the transfinite MoM was demonstrated on numerical simulations of the scattering of a TM plane wave by dielectric cylinders. Although the applications of this paper are only dealing with 2-D problems, the transfinite MoM could be generalized in the near future to the more realistic case of 3-D scatterers. In this case, the theory presented here could be advantageously applied for instance in the integral formulations presented in [4] or [13].

Appendix A

In the quadratic p version, the expansion of the electric field inside each interpolation cell $\Omega_c[0,h]\times[0,h]$ is given by (20). Thanks to (31) and (30), $\tilde{\pi}_c(x,y)$ can be explicitly written as a function of the point values of $E(x,y)$ at the interpolation nodes

$$\begin{aligned}\tilde{\pi}_c(x,y) = {} & f_{00}E(0,0) + f_{(h/2)0}\,E(h/2,0) + f_{h0}E(h,0)\\ & + f_{0(h/2)}\,E(0,h/2) + f_{h(h/2)}\,E(h,h/2)\\ & + f_{0h}E(0,h) + f_{(h/2)h}\,E(h/2,h)\\ & + f_{hh}E(h,h)\end{aligned} \tag{A.1}$$

where the expansion functions are

$$\begin{aligned}f_{00} &= -\frac{1}{h^3}\,(y-h)(x-h)(2(y-h/2)\\ &\quad +2(x-h/2)+h)\\ f_{(h/2)0} &= \frac{4x}{h^3}\,(x-h)(y-h)\\ f_{h0} &= \frac{x}{h^3}\,(y-h)\,(2(y-h/2)-2(x-h/2)+h)\\ f_{0(h/2)} &= \frac{4y}{h^3}\,(y-h)(x-h)\\ f_{h(h/2)} &= -\frac{4xy}{h^3}\,(y-h)\\ f_{0h} &= \frac{y}{h^3}\,(x-h)\,(-2(y-h/2)+2(x-h/2)+h)\\ f_{(h/2)h} &= -\frac{4xy}{h^3}\,(x-h)\\ f_{hh} &= \frac{xy}{h^3}\,(2(y-h/2)+2(x-h/2)-h)\,.\end{aligned}$$

Appendix B

The generalization of the TFI to curvilinear cells is straightforward if the theory described in [15] is used. It will be briefly outlined here in the 2-D case.

Let $\Re$ be a discretization cell whose boundary $\partial\Re$ is subdivided into four parametric curved segments. To construct a curvilinear coordinate system in $\Re$ let

$$\vec{T}(s,t) = \begin{pmatrix} x(s,t)\\ y(s,t)\end{pmatrix} \tag{B.1}$$

be an univalent mapping of the square $\Im$: $[0,h]\times[0,h]$ in the (s,t) parameters plane onto $\Re$ in the (x,y) plane, i.e., $\vec{T}$: $\Im\rightarrow\Re$ provides a unique correspondence between a point $(s,t)\in\Im$ and its image $(x(s,t),y(s,t))\in\Re$. If $\vec{F}(0,t)$, $\vec{F}(h,t)$, $\vec{F}(s,0)$, $\vec{F}(s,h)$ are the four compatible parametric curves describing $\partial\Re$, $\vec{T}(s,t)$ can be defined by

$$\begin{aligned}\vec{T}(s,t) = {} & \frac{h-s}{h}\,\vec{F}(0,t) + \frac{s}{h}\,\vec{F}(h,t) + \frac{h-t}{h}\,\vec{F}(s,0)\\ & + \frac{t}{h}\,\vec{F}(s,h) - \frac{(h-s)(h-t)}{h^2}\,\vec{F}(0,0)\\ & - \frac{st}{h^2}\,\vec{F}(h,h) - \frac{(h-t)s}{h^2}\,\vec{F}(h,0)\\ & - \frac{(h-s)t}{h^2}\,\vec{F}(0,h).\end{aligned} \tag{B.2}$$

In the TFI formalism, $\vec{T}(s,t)$ is in fact the bilinear transfinite interpolant of $\vec{F}(s,t)$ on $\Im$ and the generalization to three dimensions is thus obvious as for the interpolation process. Any

function $f(x,y)$ defined on $\Re$ corresponds to a function $f^*(s,t)$ defined on $\Im$ by the identification

$$f(x(s,t),y(s,t)) = f^*(s,t) \qquad (s,t) \in \Im. \tag{B.3}$$

The univalent mapping $\vec{T}(s,t)$ defines a curvilinear coordinate system on $\Re$ (for a complete discussion about the univalency of $\vec{T}$ see [15]) and considering this curvilinear system, (18) holds, i.e.,

$$\pi_c(s,t) = (P_s^c \oplus P_t^c)\phi(s,t) \tag{B.4}$$

is a transfinite interpolant of $\phi(s,t)$ on cell c, and all the considerations concerning the interpolation errors can be extrapolated to this more general case.

ACKNOWLEDGMENT

The author would like to thank Prof. S. Prohoroff and Y. Louis of the University of Brussels for reading this paper.

REFERENCES

[1] R. F. Harrington, *Field Computation by Moment Methods*. New York: MacMillan, 1968.
[2] W. J. Gordon, "Blending-function methods of bivariate and multivariate interpolation and approximation," *SIAM J. Numer. Anal.*, vol. 8, pp. 158–177, Mar. 1971.
[3] J. H. Richmond, "Scattering by a dielectric cylinder of arbitrary cross section shape," *IEEE Trans. Antennas Propagat.*, vol. AP-13, pp. 334–341, May 1965.
[4] R. D. Graglia, "The use of parametric elements in the moment method solution of static and dynamic volume integral equations," *IEEE Trans. Antennas Propagat.*, vol. 36, pp. 636–646, May 1988.
[5] J. C. Cavendish, W. J. Gordon, and C. A. Hall, "Ritz-Galerkin approximations in blending function spaces," *Numer. Math.*, vol. 26, pp. 155–178, 1976.
[6] A. G. Papagiannakis, "Application of a point-matching MoM reduced scheme to scattering from finite cylinders," *IEEE Trans. Antennas Propagat.*, vol. 45, pp. 1545–1553, Sept. 1997.
[7] E. Yamashita, *Analysis Methods for Electromagnetic Wave Problems*. Boston, MA: Artech House, 1990.
[8] D. T. Bishop, D. M. Sullivan, and O. M. Gandhi, "Comparison of the FFT conjugate gradient method and the finite difference time-domain method for the 2-D absorption problem," *IEEE Trans. Microwave Theory Tech.*, vol. MTT-35, pp. 383–395, Apr. 1987.
[9] K. Umashankar and A. Taflove, *Computational Electromagnetics*. Boston, MA: Arctech House, 1993.
[10] D. E. Livesay and K. Chen, "Electromagnetic field induced inside arbitarily shaped biological bodies," *IEEE Trans. Microwave Theory Tech.*, vol. MTT-22, pp. 1273–1280, Dec. 1974.
[11] D. H. Schaubert, D. R. Wilson, and A. W. Glisson, "A tetrahedral modeling method for electromagnetic scattering by arbitarily shaped inhomogeneous dielectric bodies," *IEEE Trans. Antennas Propagat.*, vol. AP-32, pp. 77–85, Jan. 1984.
[12] C. Tsai, H. Massoudi, and C. H. Durney, "A procedure for calculating fields inside arbitrarily shaped, inhomogeneous dielectric bodies using linear basis functions with the moment method," *IEEE Trans. Microwave Theory Tech.*, vol. MTT-34, pp. 1131–1138, Nov. 1986.
[13] M. F. Cátedra, E. Gago, and L. Nuño, "A numerical scheme to obtain the RCS of three-dimensional bodies of resonant size using the conjugate gradient method and the fast Fourier transform," *IEEE Trans. Antennas Propagat.*, vol. 37, pp. 528–537, May 1989.
[14] A. F. Peterson and P. W. Klock, "An improved MFIE formulation for TE-wave scattering from lossy, inhomogeneous dielectric cylinders," *IEEE Trans. Antennas Propagat.*, vol. 36, pp. 45–49, Jan. 1988.
[15] J. W. Gordon and C. A. Hall, "Transfinite element methods: Blending functions interpolation over arbitrary curved element domains," *Numer. Math.*, vol. 21, pp. 109–129, 1973.
[16] C. A. Hall, R. W. Luczak, and A. G. Serdy, "Numerical solution of steady state heat flow problems over curved domains," *ACM Trans. Math. Soft.*, vol. 2, pp. 257–274, Sept. 1976.
[17] W. J. Gordon, "An operator calculus for surface and volume modeling," *IEEE Trans. Comput. Graphics Applicat.*, vol. CGA-3, pp. 18–22, Oct. 1983.
[18] C. A. Hall and J. Heinrich, "A finite element that satisfies boundary conditions exactly," *J. Inst. Math. Applicat.*, vol. 21, pp. 237–250, 1978.
[19] L. P. Bos, J. E. Grabenstetter, and K. Salkauskas, "Pseudotensor product interpolation and blending with families of univariate schemes," *Comput.-Aided Geometric Design*, vol. 13, pp. 429–440, 1996.
[20] M. Bercovier and E. Shilat, "Enhancement of Gordon-Coons interpolation by bubble-functions," *Comput.-Aided Geometric Design*, vol. 10, pp. 253–265, 1993.
[21] J. M. Jin, V. V. Liepa, and C. T. Tai, "A volume-surface integral equation for electromagnetic scattering by inhomogeneous cylinders," *J. Electromagn. Waves Applicat.*, vol. 2, pp. 573–588, 1988.
[22] P. De Doncker, "A transfinite moment method applied to electromagnetic scattering," *Proc. PIERS'98*, vol. 2, p. 606, July 1998.

Philippe De Doncker received the Eng. degree in physics from the Université Libre de Bruxelles, Belgium, in 1996

He is currently an Assistant with the Université Libre de Bruxelles. His research interest is focused on computational electromagnetics.